Int. J. Electrochem. Sci., 13 **(2018)** 9681 – 9692, doi; 10.20964/2018.10.25

International Journal of
ELECTROCHEMICAL
SCIENCE
www.electrochemsci.org

Preparation of TiO_2 Thin Film by Two-Step Anodization and Investigation of Its Corrosion Resistance

Zhiwen Wang[1], *Ju Rong*[1,2,*], *Yannan Zhang*[1], *Xiaohua Yu*[1,2,*], *Zhaolin Zhan*[1]

[1] Faculty of Materials Science and Engineering, Kunming University of Science and Technology, Kunming 650093, P.R. China.
[2] National Engineering Research Center of Waste Resource Recovery, Kunming University of Science and Technology, Kunming 650093, P.R. China.
[*]E-mail: JRong_kmust@163.com, xiaohua_y@163.com

Received: 7 May 2018 / *Accepted:* 18 July 2018 / *Published:* 1 September 2018

A TiO_2 thin film was prepared by two-step anodic oxidation and its morphology and corrosion resistance were compared with those of a TiO_2 thin film prepared by a one-step anodization process. The micro-morphology was observed by scanning electron microscopy (SEM) and atomic force microscopy (AFM). The phase composition and valence state of the films were studied by X-ray diffraction (XRD) and X-ray photoelectron spectroscopy (XPS). In addition, the corrosion resistance behavior of the film was assessed using an electrochemical workstation. The results show that the two-step anodic oxidation effectively reduced the porosity and roughness of the film. The thickness of the film was 1.33 times higher than that of the pre-processed film, and its compactness and stability also increased. Furthermore, this process yielded a reduction in the number of channels available to Cl^- ion transport in the film. Moreover, the self-corrosion potential increased by 10.16% (from −1.28 V to −1.15 V) and the self-corrosion current density decreased by 57.86% (from 0.0513 A/cm^2 to 0.0216 A/cm^2) in a 3.5 wt.% NaCl solution.

Keywords: TA2 pure titanium; two-step anodic oxidation; micro morphology; corrosion resistance

1. INTRODUCTION

Titanium and titanium alloys have low standard electrode potential, very active chemical properties, and easily form very thin titanium dioxide films when exposed to air[1]. Although the oxide film has certain protective effects, it can easily be destroyed under mechanical stress, which greatly restricts the use of titanium[2]. At present, anodic oxidation technology has been used to prepare a homogeneous and strong anodic oxide film on the surface of titanium components, endowing them

with good resistance to corrosion and wear, and good biocompatibility[3,4]. This technology has attracted the interest of many research groups over the past years. The results obtained so far show that the performance of the anodic oxidation film mainly depends on its microstructure, phase composition and thickness, which are all closely related to the preparation process[5,6]. For example, titanium oxide has been used to improve the biocompatibility of membranes by favoring the deposition of a layer of phosphorus, the main element present in human bones. Increasing the thickness of the oxide film can effectively increase the corrosion and wear resistance of titanium and its alloys[7]. The anodized film has a porous structure, mainly composed of anatase titanium dioxide and rutile titanium dioxide, and has an environmental photocatalytic effect. It has potential for application in the fields of medical materials and environmental control[8,9].

At present, the simple anodizing process on the surface of titanium and its alloys has reached some degree of industrialization. But the single-step anodizing technology has certain limitations in terms of color, thickness and microstructure control of the film and therefore cannot fully meet material requirements[10]. More specifically, there is still a lot of room for improvement in corrosion resistance, wear resistance and biocompatibility. It has been noticed that the anodic oxidation technology of aluminum alloys shares many characteristics with that of titanium alloys. Combining knowledge on the porous structure of aluminum alloys and of its two-step oxidation[11,12], while neglecting the more uncertain factors regarding the electrolysis system, may provide insight on the development of new functional materials, characterized by good compactness and stability, as well as low solar absorptivity and high solar radiation rates. Despite the good practicability of this route, titanium alloys have still not received enough attention in this area[13].

On the basis of the ideas presented above, this paper studies the anodization of TA2 titanium sheets using an H_2SO_4 solution as electrolyte and different pressurization methods. The effect of different compression methods on the passivation film formed on the titanium surface was studied by scanning electron microscopy (SEM), X-ray photoelectron spectroscopy (XPS), and electrochemical workstation, so as to provide reference information for different applications of titanium and its alloys.

2. EXPERIMENT

2.1 Experimental method

A TA2 pure Ti sample (dimensions: 100 mm × 100 mm × 2 mm), with composition shown in Table 1, was used as the base material for the experiments.

Table 1. Chemical composition of TA2 industrially pure titanium

Element	Fe	C	N	H	O	Ti
Mass fraction/%	0.35	0.17	0.03	0.014	0.33	Bal

The experimental procedure consisted initially in cleaning the titanium sheets under ultrasonic conditions with acetone, alcohol, and deionized water in turn. The sheets were then anodized, with the

titanium plate acting as the anode and the graphite plate as the cathode. The surface ratio between the anode and cathode plate was 3:1, the spacing between the plates was 5 cm, the electrolyte solution was 0.5 M H_2SO_4, and the operating temperature was 25°C. The first group of samples was treated by anodic oxidation at a voltage of 40 V and the treatment time was 360 s. These samples were designated as Ti_{40}. The second group of samples was treated with two-step anodization. The first treatment lasted 180 s at 30 V and the second treatment lasted 180 s at 40 V. The samples will be referred to as $Ti_{30\text{-}40}$.

2.2 Detection Techniques

The micromorphology of the sample was observed via SEM (LEO 1530Vp, Germany) performed at an acceleration voltage of 15 kV. Furthermore, X-ray diffraction (XRD, D8 ADVANCE Germany; radioactive source: Cu Kα=1486.6 eV, λ = 0.15406 nm), with operating voltage and current of 30 kV and 30 mA, respectively, was used to determine the crystallinity and stability of the oxide film. Moreover, XPS (PHI5000 Versaprobe-II Germany) was used to analyze the element composition and changes in the valence state of the film. The anode was an Al target (hv = 1486.6 eV).

An electrochemical workstation (HI660E, Shanghai) was used to investigate the corrosion resistance behavior of the samples. In the three-electrode system, Pt and a saturated calomel electrode were used as the counter electrode and the reference electrode, respectively. Tests were performed at a temperature of 27±0.1°C, and a potential scanning rate of 0.03 mV/s. The potentiodynamic polarization test was performed after the sample was soaked for 1h in a 3.5 wt.% NaCl solution. In addition, the electrochemical impedance spectroscopy (EIS) measurements were performed under open circuit potential. The electrochemical experiments were all repeated five times to ensure the accuracy of the measurement.

3. RESULTS AND DISCUSSION

3.1 Microlayer morphology analysis

Figure 1 shows the microstructure of the oxide films formed on the Ti_{40} (a, b) and $Ti_{30\text{-}40}$ (c, d) samples at different magnifications. It can be seen from Fig. 1(a, b) that a large number of irregularly shaped holes with a size of 5–10 nm are distributed on the surface of the Ti_{40} sample with high porosity. Compared to the Ti_{40} sample, the number of holes on the surface of the $Ti_{30\text{-}40}$ (c, d) sample is significantly lower. In addition, the depth of the holes is also reduced (Fig. 1b, d). The Image J software was used to determine the hole number and porosity of Ti_{40} and $Ti_{30\text{-}40}$. The hole number was found to be 45 and 16, respectively. And the porosity was 18.6% and 6.1%, respectively. This indicates that the secondary anodization can significantly improve the surface morphology of the anodized film and reduce the porosity of the sample surface, thereby increasing the density and stability of the film layer.

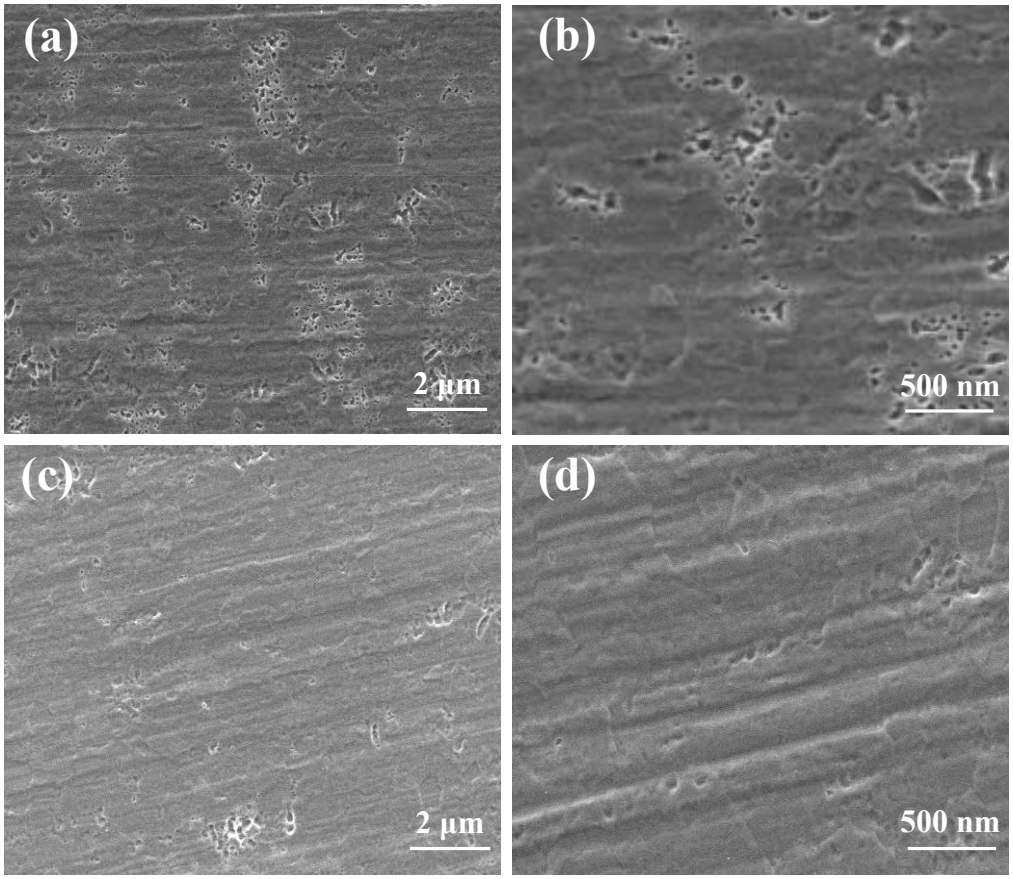

Figure 1. Micrograph of surface oxide films on Ti_{40} (a, b) and $Ti_{30\text{-}40}$ (c, d) samples

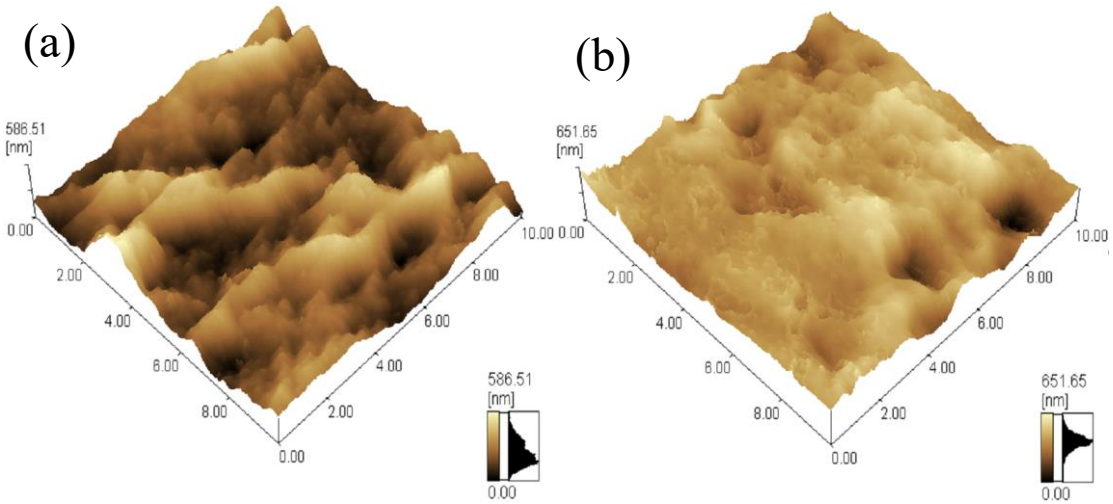

Figure 2. AFM Figure of (a) Ti_{40} and (b) $Ti_{30\text{-}40}$ samples surfaces

Surface roughness is an important characteristic of the oxide film and significantly affects its properties. In order to investigate the effect of secondary anodization on the surface roughness of the oxide film, the average surface roughness (R_a) and root mean square of the sample roughness (R_{ms}) were obtained by three-dimensional atomic force microscopy (AFM). It can be seen from Figure 2 that

the R_a and R_{ms} of the oxide film on the surface of the Ti_{40} sample are 43.5 and 57.4, respectively. While the corresponding values on $Ti_{30\text{-}40}$ sample are 35.6 and 41.2, respectively. Which indicats that the roughness of the oxide film was reduced after the secondary anodization step, in agreement with the observed decrease in porosity of the sample surface.

3.2 Film phase composition and surface valence analysis

Figure 3 shows the XRD patterns of oxide films formed on the Ti_{40} and $Ti_{30\text{-}40}$ samples. From the figure, it can be seen that the oxide films mainly consist of anatase TiO_2 and $Ti(OH)_4$. Ti diffraction peaks appear at 2θ values of 40.18°, 54.34°, and 76.3°[13]. The film thickness is less than the X-ray detection depth (< 35 μm) and therefore a characteristic peak corresponding to substrate Ti also occurs in the pattern, indicating that the secondary anodic oxidation does not change the phase of the oxide film[14,15]. The intensity of the TiO_2 diffraction peaks in the anatase and rutile phases increases on the surface of $Ti_{30\text{-}40}$ samples, but the intensity of the diffraction peaks on the Ti substrate decreases, which may be related to changes in the thickness of the oxide film. The thickness of the surface layer increases following the secondary anodization step, and the XRD's acceptance of diffracted waves on the substrate becomes weaker[16].

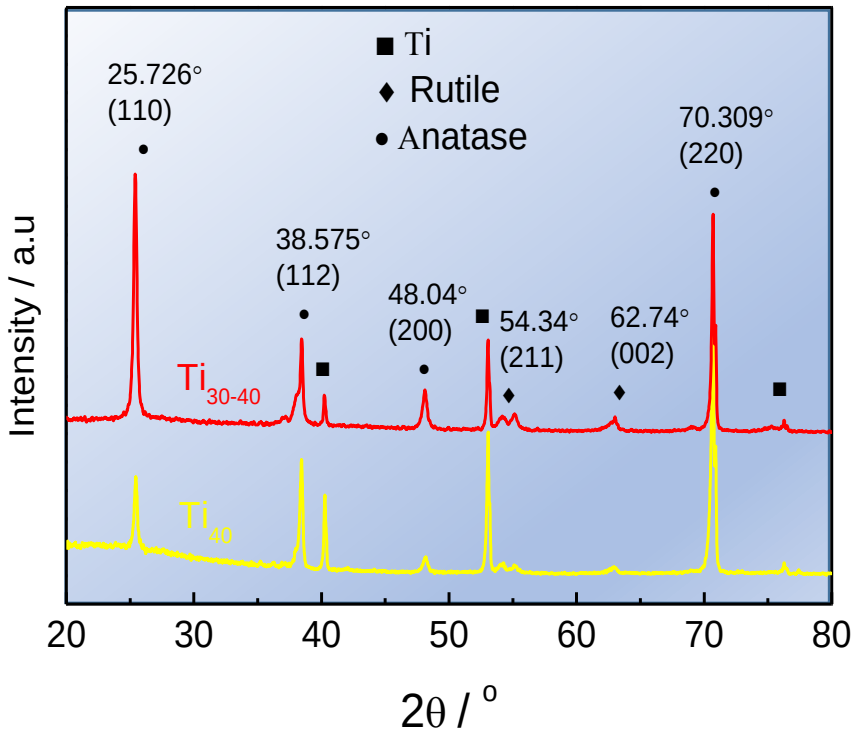

Figure 3. Phase composition of Ti_{30} and $Ti_{30\text{-}40}$ samples.

The thickness of the anodic oxide film has a great influence on the corrosion and wear resistance of titanium and its alloys. In order to further verify the effect of secondary anodic oxidation on the thickness of the oxide film layer, the film thickness of the sample was measured by the XPS deep sputtering method. The deep sputtering process was carried out from the surface of the sample to

the inside of the substrate, and the disappearance of the oxide film was assumed when the atomic percentage of oxygen reached 0. From the deep sputter patterns of the Ti_{40} and $Ti_{30\text{-}40}$ samples (Fig. 4), it can be seen that as the depth of sputtering increases, the Ti element content continuously increases, and the O element content continuously decreases. The content of O on the surface of the Ti_{40} and $Ti_{30\text{-}40}$ reaches the value of 0 for depth of sputtering times of 9 and 12 min, respectively. Since the measurements had been carried out at a sputtering speed of 30.4 nm/min[17], the thicknesses of oxide films on the surfaces of Ti_{40} and $Ti_{30\text{-}40}$ were calculated to be 273.6 and 364.8 nm, respectively. This result shows that under constant electrolyte system and electrolysis time, the secondary anodization can significantly increase the thickness of the film, which is consistent with the results of the XRD analysis.

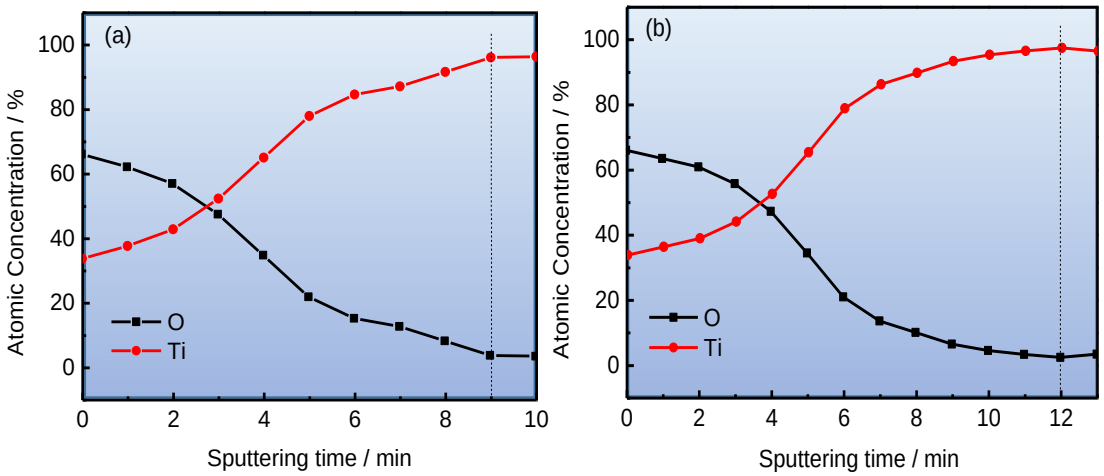

Figure 4. Depth analysis of sputtering of oxide films for the Ti_{40} and $Ti_{30\text{-}40}$ samples

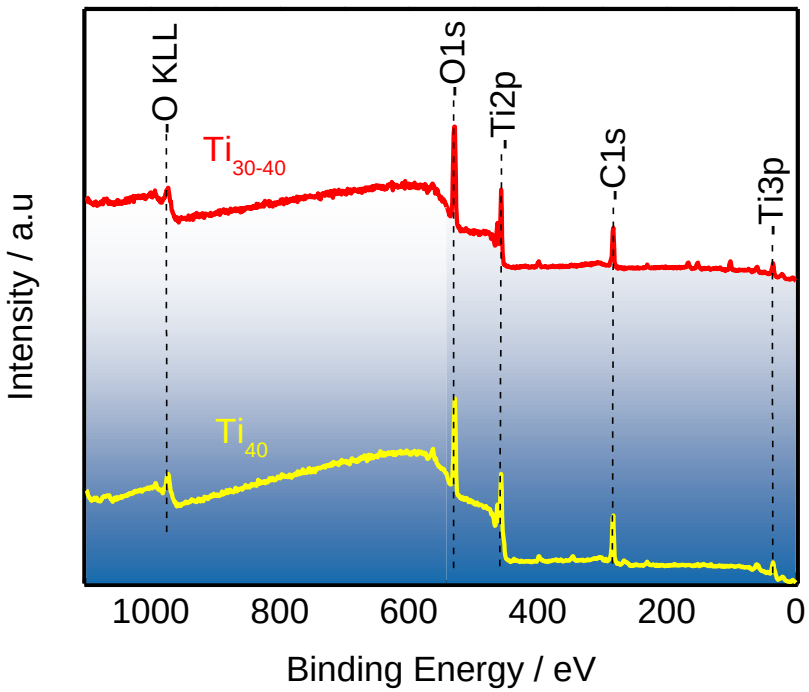

Figure 5. XPS wide spectra of the Ti_{40} and $Ti_{30\text{-}40}$ samples

In order to obtain the chemical composition of the oxide film on the surface of the sample, XPS analyses were performed on the Ti_{40} and $Ti_{30\text{-}40}$ samples. The full spectrum of the oxide films formed on the surfaces of the Ti_{40} and $Ti_{30\text{-}40}$ samples (Figure 5) reveals that the surface of the samples is mainly composed of C, N, Ti, and O. The detailed composition is shown in Table 2. The presence of C and N is due to pollution. A comparison of the compositions of the two oxide films reveals that the O content is higher on the surface of $Ti_{30\text{-}40}$. The excess oxygen contributed to increase the sample's degree of oxidation and thus increased the overall density of the film.

Table 2. Chemical composition of oxide films formed on the Ti_{40} and $Ti_{30\text{-}40}$ samples

Sample	Elemental content (at.%, Mean±SD)			
	C	N	O	Ti
Ti_{40}	2.75±0.12	0.98±0.16	42.98±0.56	53.62±0.42
$Ti_{30\text{-}40}$	2.52±0.53	1.06±0.69	46.79±0.37	49.87±0.19

The valence states of the elements in the oxide film were further analyzed by XPS analysis. Figures 6(a) and (b) show the Ti2p narrow spectrum of the oxide films formed on the Ti_{40} and $Ti_{30\text{-}40}$ samples, respectively. The Ti2p spectra of both samples consist of two pairs of overlapping peaks. The binding energies of the peaks located at $BE_{Ti2p1/2}$=457.02 eV, $BE_{Ti2p3/2}$=462.58 eV, $BE_{Ti2p1/2}$=457.63 eV, and $BE_{Ti2p3/2}$=463.26 eV and were correspond to Ti^{4+}[18]. This result shows that the surface oxide film is mainly composed of stable Ti^{4+}. The secondary anodic oxidation does not change the valence composition of Ti in the oxide film.

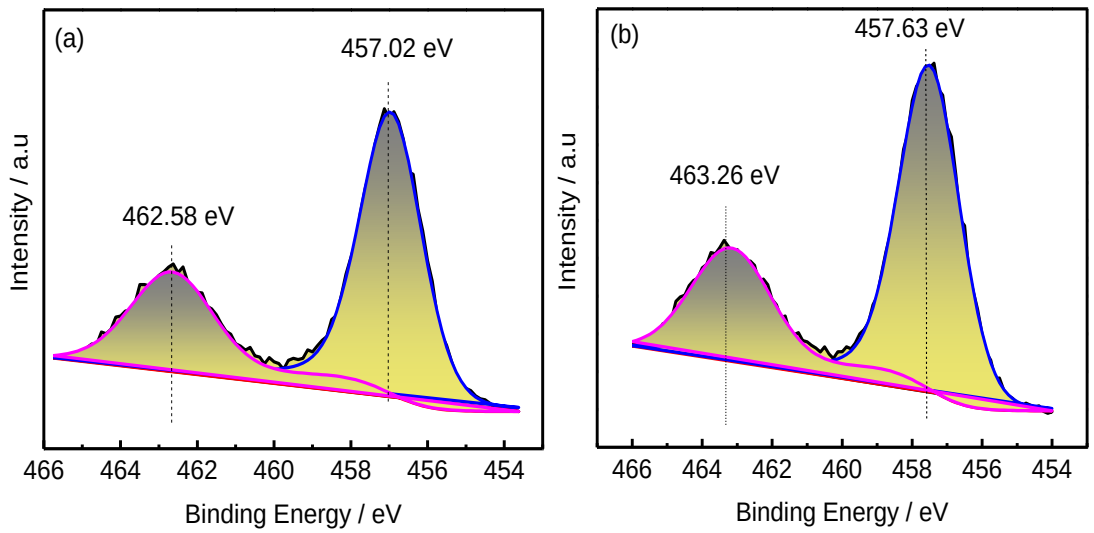

Figure 6. Ti2p XPS spectra of the oxide film formed on the Ti_{40} (a) and $Ti_{30\text{-}40}$ (b) samples

Figures 7(a) and (b) are the O1s narrow spectra of the oxide films formed on Ti_{40} and $Ti_{30\text{-}40}$, respectively. It can be seen from the figure that the O1s spectra of the two samples consist of two pairs of overlapping peaks, and the binding energies were located at $BE_{Ti2p1/2}$=530.96 eV and $BE_{Ti2p3/2}$=530.95 eV for O^{2-}[19], $BE_{Ti2p1/2}$=531.76 eV, $BE_{Ti2p3/2}$=531.74 eV for OH^-[20], and $BE_{Ti2p1/2}$=533.54 eV, $BE_{Ti2p\ 3/2}$=533.34 eV for H_2O bonded to the oxide films[21]. The valence state

composition of the two samples revealed that their main surface components remain TiO_2 and $Ti(OH)_4$, even after the secondary anodization step, consistently with the XRD results. The relative content of O^{2-}, OH^-, and H_2O in the oxide films can be calculated based on the area of each overlapping O1s peak, as shown in Table 3. Which shows that the O^{2-} content in the oxide film on the surface of the Ti_{30-40} sample is significantly higher than that on the surface of the Ti_{40} sample. While the relative content of OH^- and H_2O is significantly reduced. Studies have shown that OH^- and surface-bound water are the main reasons for the formation of amorphous Ti[22,23]. Secondary anodization reduces the relative content of OH^- and H_2O in the oxide film, which is conducive to the formation of a stable anatase TiO_2 in the oxidation process and improves the stability of the oxide film.

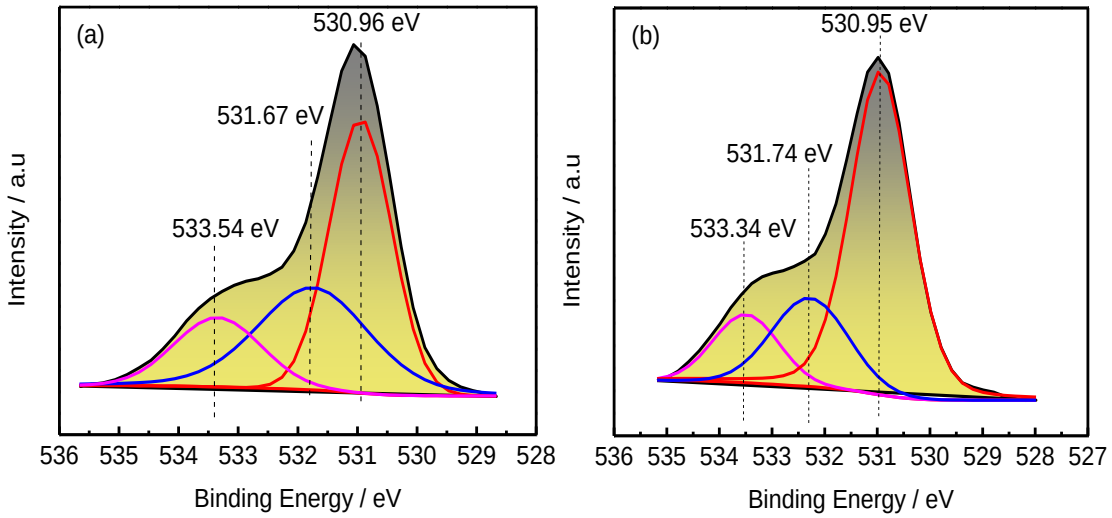

Figure 7. O1s XPS spectra of the oxide film formed on the Ti_{40} (a) and Ti_{30-40} (b) samples

Table 3. Relative O^{2-}, OH^-, and H_2O content of the oxide film formed on the Ti_{30} and Ti_{30-40} samples

Samples	Contribution of O1s components（%）		
	O^{2-}	OH^-	H_2O
Ti_{30}	68.73	32.19	5.12
Ti_{30-40}	75.69	26.35	4.67

3.3 Corrosion resistance analysis

Figures 8(a) and (b) show, respectively, the polarization and Tafel curves of the Ti_{40} and Ti_{30-40} samples in the 3.5 wt.% NaCl solution at room temperature. As shown in Fig. 8(a), both samples noticeably display passivation. The cathodic region of the polarization curve is mainly due to the hydrogen evolution reaction. After a short dissolution of the anodic zone, a dense passivation film is formed on the surface of the sample, resulting in the passivation of the metal. The passivation current density (j_{pass}) of the sample can be obtained from the polarization curve, as shown in Table 4. According to Zhou[24], an increase in the intensity of the passivation current density reflects a decrease in the stability of the oxide film. Table 4 shows that the j_{pass} value of on Ti_{30-40} sample is

significantly lower than the one on Ti_{40}, indicating that the two-step anodic oxidation improves the stability of the oxide film and the resistance to Cl^- corrosion.

The electrochemical parameters, such as self-corrosion potential (E_{corr}), self-corrosion current density (j_{corr}), cathodic polarization slope (β_c) and anodic polarization slope (β_a)[25,26], can be obtained from the Tafel curve shown in Fig. 8(b) and are reported in Table 4. The value of E_{corr} reflects the corrosion tendency of the materials. The greater the value, the less corrosive the material. By comparing the self-corrosion potentials, it is found that the $Ti_{30\text{-}40}$ sample is less susceptible to corrosion than Ti_{40} in a 3.5 wt.% NaCl solution. As the Tafel curve experienced a cathodic polarization process before reaching E_{corr}, the surface of the passivation film was destroyed. A lower β_c indicates that the material has higher corrosion resistance. While a lower β_a indicates that the anodic dissolution of the material occurs more easily. Comparing the polarization slope of the two samples, it is found that the β_a of the Ti_{40} sample is lower, indicating that the electrochemical reaction is controlled by the anodic process. The β_c of $Ti_{30\text{-}40}$ is lower. The electrochemical process is controlled by cathodic process, and $Ti_{30\text{-}40}$ has a higher corrosion resistance. The j_{corr} value reflects the rate of corrosion: a higher values is indicative of a higher corrosion rate[27]. It was found that the two-step anodic oxidation causes a decrease in the j_{corr} value, indicating that the corrosion rate of $Ti_{30\text{-}40}$ is significantly lower than that of Ti_{40}.

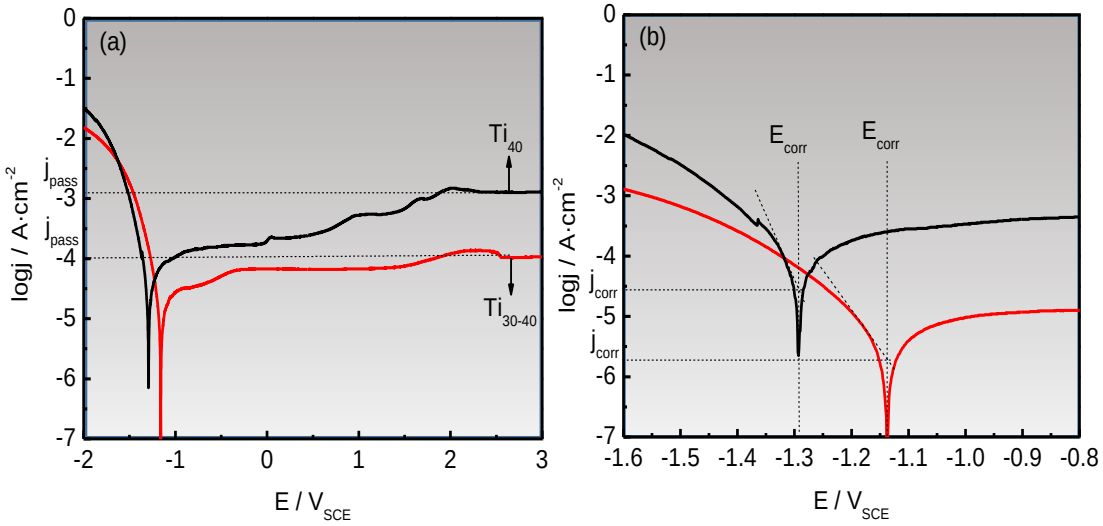

Figure 8. Potentiodynamic polarization curves of the oxide films formed on the samples

Table 4. Polarization curve data of the samples immersed in a 3.5 wt.% NaCl solution

Sample	j_{pass}/A.cm^{-2}	E_{corr}/V$_{SCE}$	j_{corr}/A.cm^{-2}	β_a/ mV.dec^{-1}	β_a/ mV.dec^{-1}
Ti_{40}	1.38×10^{-3}	−1.28	0.0513	128	−95
$Ti_{30\text{-}40}$	5.86×10^{-5}	−1.15	0.0216	152	−91

Electrochemical impedance spectroscopy (EIS) can be used to obtain the intrinsic properties of the passive film and the electrochemical reaction process. Figure 9 shows the Nyquist and Bode diagrams of the anodic oxidation film on the surface of the Ti_{40} and $Ti_{30\text{-}40}$ samples in the 3.5 wt.% NaCl solution at 27°C. It can be seen that the capacitance resistance of the $Ti_{30\text{-}40}$ sample is larger than

that of the Ti_{40} sample (Fig. 9(a)). The circular curve reflects the charge transfer process of the electrode surface. The larger the arc diameter, the greater the electron transfer resistance, and the stronger the stability of the oxide film. The curve indicates that the oxide film on the surface of the $Ti_{30\text{-}40}$ sample acts as a stronger barrier against the corrosive medium.

The surfaces of the Ti_{40} and $Ti_{30\text{-}40}$ samples showed typical single time constants (Fig. 9(b)). In the high frequency region (10^3–10^5 Hz), the phase angle increases with decreasing frequency as a consequence of the electrolyte reaction. In the intermediate frequency region (1–10^3 Hz), the phase angle remains virtually constant. In the low frequency region (0.01–1 Hz), the phase angle decreases with decreasing frequency, and the surface exhibits typical passivation reaction characteristics[28,29].

In the 3.5 wt.% NaCl solution, the phase angle value of the $Ti_{30\text{-}40}$ sample in the low frequency region is obviously higher than that of the Ti_{40} sample. In the intermediate frequency region, the phase angle peak of the $Ti_{30\text{-}40}$ sample is obviously widened relative to the Ti_{40} sample and approaches 90°. According to Jamesh[30], a higher phase angle is characteristic of samples with higher corrosion resistance, indicating that the formation of a passivating film on the $Ti_{30\text{-}40}$ sample in the NaCl solution is fast. The film has a good isolation and permeation effects, hindering the diffusion and migration of the corrosive medium and increasing the impedance, thus improving the corrosion resistance. Therefore, the stability of the oxide film formed on the $Ti_{30\text{-}40}$ sample is improved, the charge transfer is reduced, and the ability to resist Cl^- corrosion is increased.

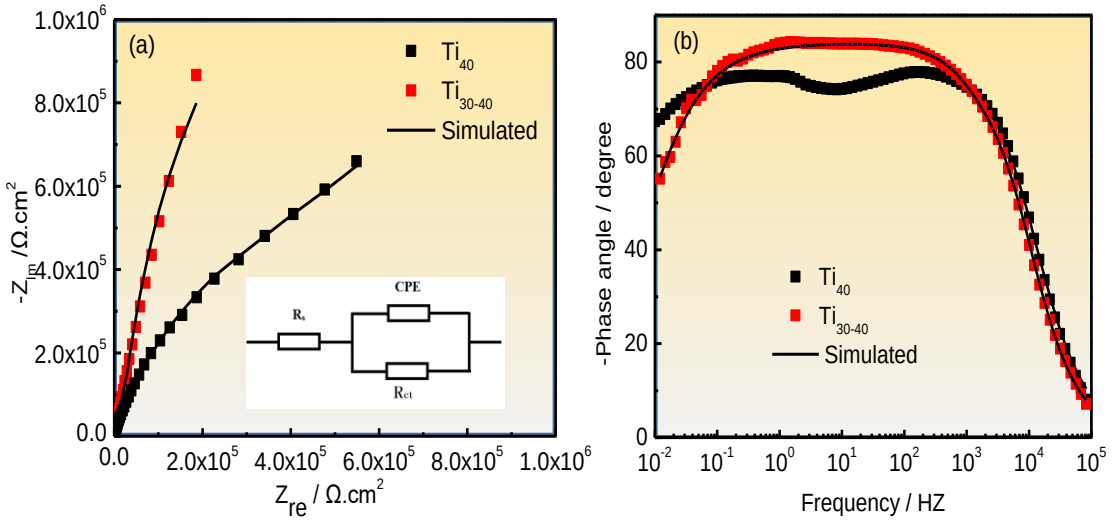

Figure 9. Nyquist and Bode diagrams of the (a) Ti_{40} and (b) $Ti_{30\text{-}40}$ samples immersed in a 3.5 wt.% NaCl solution at 27 °C.

Since only one time constant can be obtained from the phase map, the surface electrochemical impedance spectrum of the sample in 3.5 wt.% NaCl solution was fitted by the Randle equivalent circuit containing the time constant, as illustrated in Figure 9(a). R_s indicates the solution resistance. CPE represents the double layer capacitance on the surface of the working electrode. R_{ct} represents the charge transfer resistance of the working electrode. And Z_w represents the diffusion resistance, which is used to reflect the diffusion behavior of the vacancy during the formation of the passivation

film[31,32]. The values of the parameters of each circuit element obtained from the fitting procedure are shown in Table 5.

Table 5. EIS fitting circuit parameters of the Ti_{40} and $Ti_{30\text{-}40}$ samples immersed in a 3.5 wt.% NaCl solution

Sample	R_s/（Ω·cm^2）	CPE/（μF·cm^2）	Z_w/（kΩ·cm^2）	R_{ct}/（Ω·cm^2）
Ti40	1.13	8.32×10-3	153.6	5.76×104
Ti30-40	1.15	5.36×10-3	118.5	7.94×105

In the corrosion solution, the passivation film characteristics and corrosion resistance of the material are mainly determined by the charge transfer resistance of the working electrode. A higher R_{ct} value corresponds to a strong corrosion resistance and its decrease indicates a reduction in the protective efficiency of the barrier layer. The R_{ct} of the coating obtained by two-step anodization increases and reaches 7.94×10^5 Ω·cm^2, which is 14 times higher than the corresponding value for Ti_{40}. The results indicate the obvious improvement of the corrosion resistance and protective effect obtained by carrying out the two-step anodization process.

4. CONCLUSIONS

TA2 was anodized in a 0.5M H_2SO_4 system. The oxide film thus obtained was porous. After a two-step anodization process, its thickness increased by 91.2 nm, corresponding to a 1.33-time increase. And the surface morphology became more compact. With a decrease in the number of pores, overall porosity is reduced by 12.5%. The phase composition of the film was not affected by the two-step anodic oxidation. The main components in the passivation films of Ti_{40} and $Ti_{30\text{-}40}$ were always $Ti(OH)_4$ and TiO_2, but the amorphous Ti content in the $Ti_{30\text{-}40}$ film layer was lower. The stability of the film is improved.

The corrosion resistance is correlated to the surface microstructure. The dense oxide film structure on the surface of $Ti_{30\text{-}40}$ reduces the void defect of the film and, consequently, the channel available for the transmission of Cl^- ions. In the 3.5 wt.% NaCl solution, the self-corrosion potential is increased from −1.28 V, without mechanical grinding, to −1.15 V, corresponding to a 10.16% increase, and the corrosion current density decreased from 0.0513 A/cm to 0.0216 A/cm, corresponding to a 57.89% decrease.

ACKNOWLEDGEMENTS
The authors are thankful for foundation support (NO 51601081 and 51665022).
We thank International Science Editing (http://www.internationalscienceediting.com) for editing this manuscript.

References

1. M.J. Jackson, J. Kopac, M. Balazic, W. Ahmed. *Int. J. Nano. Biomat*., 1 (2016) 3.

2. N.X. Ya, X.X. Jing, S.X. Lan, Z.T. Feng, L. Min, Z.L, Hua. *Rare Metal.*, 43 (2014) 241.
3. I. Milošev, D. Blejan, S. Varvara, L.M. Muresan. *J. Appl. Electrochem.*, 43 (2013) 645.
4. F. Mohammadpour, M. Moradi. *Mat. Sci. Semicond. Process.*, 39 (2014) 255.
5. M.A. Baker, S.L. Assis, O.Z. Higa, I. Costa. *Acta Biomater.*, 5 (2009) 63.
6. R.K. Hart, J.K. Maurin, *Surf. Sci.*, 20 (1970) 285.
7. L. Benea, E. Danaila, P. Ponthiaux. *Corros. Sci.*, 91 (2015) 262.
8. C. Qi, L. Cheng, M. Kun, Y.X. Hua, Z.Y. Nan, L.J. Xiong, J. Xin, J.L. Ying. *Int. J. Electrochem. Sci.*, 13 (2018) 265.
9. W.Z. Wen, D.R. Jia, Y.Z. Tao, Y.X. Hua, F.T. Lin, Z. Yan, Z.Z. Lin. *Int. J. Electrochem. Sci*, 13 (2018) 4411.
10. F.T. Lin, Z.Z. Lin, Z. Ling. *Trans. Mater. Heat Treat.*, 35 (2014) 207.
11. W. Simka. *Electrochim Acta.*, 56 (2011) 8962.
12. F. Nasirpouri, M. Abdollahzadeh, M.J. Almasi, N. Parvini. *Curr. Appl. Phys.*, 9 (2009) S91.
13. H.X. Wen, L.Z. Jian. *Surf. Coat. Tech.*, 232 (2013) 224.
14. B.J. Wei, Z.X. Tao, W.Z. Guo, H.X. Quan, L.Y. Ling, F.X. Dong. *J. Sichuan Univ. Nat. Sci.*, 41 (2004) 995.
15. W. Xiao, R. Ju, S.Y. Min, Y.X. Hua, Z.Z. Lin, D.J. Shuai. *Phys. Lett. A*, 381 (2017) 2845.
16. M.H. Yao, R.J. Baird, F.W. Kunz. T.H. Hoost. *J. Catal.*, 166 (1997) 67.
17. L. Yan, Z.T. Ting, W.S. Bo, X. Yan. *Mater. Sci. Eng. C*, 30 (2010) 1227.
18. H. Satoshi, T. Akihiro. *Surf. Interface Anal.*, 34 (2010) 262.
19. I. Milošev, T. Kosec, H.H. Strehblow. *Electrochim. Acta*, 53 (2008) 3547.
20. N.T.C. Oliveira, A.C. Guastaldi. *Acta Biomater.*, 5 (2009) 399.
21. F.T. Lin, W. Xiao, L.J. Xiong, L. Li, Y.X. Hua, Z.Z. Lin. *JOM.*, 69 (2017) 1844.
22. X.Z. Bin, N. Hiroshi, T. Hiroyuki, E. Takeo, I. Miki, F. Motoaki, O. Jun. *Electrochem. Commun.*, 9 (2007) 850.
23. B.J. Hwang, J.R Hwang. *J. Appl. Electrochem.*, 23 (1993) 1056.
24. Z.C. Lu, L. Xin, X. Zhong, L. Juan. *Corros. Sci.*, 70 (2013) 145.
25. S.L.D. Assis, S. Wolynec, I. Costa. *Electrochim. Acta*, 51 (2006) 1815.
26. W.G. Song, D.K. Jian, Z.X. Qing, W.X. Min, Y.S. Shan. *Scr. Mater.*, 61 (2009) 269.
27. X.F. Xia, H.X. Bo, C.S. Li,M. Min, Q.X. Hui. *Electrochim. Acta*, 105 (2013) 121.
28. M.A. Khan, R.L. Williams, D.F. Williams. *Biomaterials*, 20 (1999) 631.
29. M. Fazel, H.R. Salimijazi, M.A. Golozar, H.M. Garsivazjazi. *Appl. Surf. Sci.*, 324 (2015) 751.
30. J.M. Ibrahim, L. Penghui, B. Marcela, R.L. Boxman, M.R. David. *Corros. Sci.*, 97 (2015) 126.
31. W.Z. Wen, D.R. Jia, F.T. Lin, Y.Z. Tao, Y.X. Hua, Z.Z. Lin. *Trans. Mater. Heat Treat.*, 5 (2018) 100.
32. E.M. Szesz, C.E.B. Marino, H.A. Ponte, F.C.N. Borges. *Key Eng. Mater.*, 396 (2009) 381.